LUMBAR LOCOMOTOR-RELATED V3 INTERNEURONS PROVIDE DIRECT EXCITATORY SYNAPTIC INPUT ONTO THORACIC SYMPATHETIC PREGANGLIONIC NEURONS

Camila Chacon, Chioma V Nwachukwu, Narjes Shahsavani, Kristine C Cowley and Jeremy W Chopek

Spinal Cord Research Centre, Department of Physiology and Pathophysiology, Rady Faculty of Health Sciences, University of Manitoba, Winnipeg, Manitoba, Canada, R3E 0J9

Running head title: Intraspinal synaptic input from motor to sympathetic networks

Number of words in manuscript: 9286

Number of tables: 0

Number of figures: 7

Keywords: spinal interneurons, sympathetic preganglionic neurons, motor systems, optical stimulation, propriospinal neurons

Table of contents categories: Neuroscience

Correspondence should be addressed to:

Jeremy W Chopek

Department of Physiology and Pathophysiology

Rady Faculty of Health Sciences, University of Manitoba

406- 745 Bannatyne Avenue, Winnipeg, Manitoba, CANADA R3E 0J9

Phone: (204) 789-3855

Email: Jeremy.Chopek@umanitoba.ca

Orcid: 0000-0002-4057-4389

Key points (150 words max, 3 -5 points)

- We provide direct anatomical and electrophysiological evidence of an ascending intraspinal synaptic connection between lumbar motor and thoracic sympathetic autonomic neural systems.
- These connections are formed between locomotor related V3 interneurons and thoracic sympathetic preganglionic neurons (SPNs)
- V3 synaptic input accounts for 20% of glutamatergic input to SPNs.
- Optical activation of lumbar V3 interneurons elicit action potentials in thoracic SPNS.
- This intraspinal pathway may explain why spinal electrical stimulation of the lumbar and sacral regions improved both motor and sympathetic function ins in persons with long-standing motor complete spinal cord injury

Abstract (250 words)

Spinal cord injury (SCI) is a life-altering event causing sensation loss, motor paralysis and impaired autonomic function. Spinal cord stimulation has demonstrated promise in restoring lost motor function and also impaired autonomic function, despite targeting lumbar locomotor networks. Sympathetic preganglionic neurons (SPNs), primarily located in the intermediate laminae of thoracic and upper lumbar segments indirectly excite sympathetic tissues and organs that provide homeostatic (e.g., blood pressure regulation) and metabolic support during movement and exercise. We hypothesized that ascending propriospinal neurons located in the lumbar spinal cord innervate thoracic SPNs, allowing for both improved motor and autonomic function in response to spinal cord stimulation. We demonstrate that synaptic contacts from locomotor-related V3 interneurons (INs) are found in all thoracic intermediate laminae. Injection of anterior grade tracer BDA into individual lumbar segments established a topographical organization of synaptic input to thoracic SPNs. That is, V3 INs located in high lumbar segments have a greater projection to upper thoracic SPNs and that V3 INs located in lower segments, have a greater projection to lower thoracic SPNs. We then optically stimulated V3 INs while performing whole-cell patch clamp recordings from thoracic SPNs. In thoracic slice preparations, optical activation of V3 terminals elicits action potentials in SPNs. Similar, in whole cord preparation, optical stimulation of lumbar V3 INs, elicit action potentials in SPNs. This work demonstrates a direct intraspinal link between lumbar locomotor and thoracic sympathetic networks.

INTRODUCTION

Spinal cord injury (SCI) is a life-altering event, resulting in the loss of sensation and motor paralysis. In addition, persons living with SCI face a lifetime of impaired automatic (autonomic) bodily functions that affect every aspect of daily living. These impairments include reduced temperature and blood pressure (BP) regulation, and inability to activate sympathetic nervous system responses needed during movement and exercise (e.g., increased heart rate (HR), activation of adrenal glands). Insufficient activation of spinal autonomic neural circuitry contributes to obesity, cardiovascular disease, type II diabetes and muscle and bone deterioration that fuels an estimated $1.5 – 4.6 million per person in health costs after SCI (Duckworth et al., 1980; Biering-Sorensen et al., 1990; Bauman and Spungen, 2000; Biering-Sorensen et al., 2009; de Groot et al., 2010; Noonan et al., 2012). Spinal stimulation has emerged as a powerful therapeutic to improve motor function after SCI even when applied years after injury.

A second critical yet unanticipated set of observations that emerged was that electrical stimulation targeting lower limb motor centres (lumbar SC), also improved many autonomic body functions mediated by spinal sympathetic neurons located in the thoracic spinal cord. Specifically, investigators using spinal stimulation to improve stepping and walking began reporting improved blood pressure (BP) and temperature regulation, whole body metabolism and even peak upper body exercise performance, despite the stimulation being applied to lumbar locomotor regions (reviewed by Cowley (Flett et al., 2022b)). Normally, these autonomic sympathetic preganglionic neurons (SPNs) of the thoracic SC are controlled by autonomic neurons in the brainstem. This constellation of sympathetic functions also happens to be those needed to meet the increased metabolic and homeostatic demands of exercise. In the field of

exercise physiology, this is termed ‘central command’, where brainstem nuclei activate thoracic SPNs and ensure appropriate activation of homeostatic and metabolic tissues (e.g., heart, smooth muscle of the vasculature and adrenal glands) in parallel with locomotor commands, that initiate and maintain movement and exercise.

As these movement-related sympathetic functions are improved in people with SCI during lumbar spinal electrical stimulation, it suggests intraspinal, ascending neural connections between lumbar locomotor and thoracic sympathetic neural circuitry become activated. We have previously demonstrated it was possible for completely intraspinal (propriospinal) neurons to relay descending locomotor commands from the brain (Cowley et al., 2008, 2010). Further, during fictive locomotion, the lumbar spinal cord is capable of entraining both thoracic (Le Gal et al., 2016) and cervical (Juvin et al., 2012) ventral root activity via propriospinal neurons. Thus, we thought to investigate how and what classes of propriospinal neurons could be responsible for coordinating locomotor and sympathetic function.

Studies in the early 2000s revealed that all neurons within the mouse spinal cord arise from 11 progenitor domains, 5 located in the ventral and 6 in the dorsal horn (Jessell, 2000). Based on expression of distinct transcription factor profiles among these spinal neuron populations, multiple genetic mouse models have been developed. These genetic models allow targeting specific neuronal populations (and subpopulations) which can then be visualized and manipulated to determine their role(s) in locomotion [reviewed in (Alaynick et al., 2011; Kiehn, 2016)]. We focused on the V3 population of spinal neurons because the V3 population of interneurons (INs) are important for stabilizing the frequency of locomotion (Zhang et al., 2008) and are excitatory, glutamatergic and project both ipsilaterally and contralaterally (Zhang et al., 2008; Blacklaws et al., 2015; Chopek et al., 2018a). Computational modeling suggests that V3

INs promote left-right synchrony (i.e., gallop) during high-speed locomotion and have ascending projections from lumbar to cervical regions, providing an anatomical basis for this coordination (Rybak et al., 2015; Danner et al., 2016; Danner et al., 2017; Danner et al., 2019; Zhang et al., 2022). Here we demonstrate a direct intraspinal neural connection between spinal locomotor related V3 neurons in the lumbar spinal cord and thoracic SPNs. Preliminary results presented previously in abstract and thesis form.

METHODS

Animals

Experimental protocols used complied with the guidelines set by the Canadian Council on Animal Care and were approved by the University of Manitoba animal ethics committee. Anatomical and immunohistochemical observations of V3 soma and nerve terminals, BDA and CTB injections were performed in 9 adult $Sim1^{Cre/+}$;$Rosa26^{floxstopTdTom/+}$ (Sim1TdTom; Zhang et al., 2008) mice of both sexes. Adult female and male $Sim1^{Cre/+}$;$Rosa26^{floxstopTdTom/+}$ mice were crossed with Ai32 mice (Gt(Rosa)26floxstopH134R/EYFP/+, Jackson Laboratory, Stock No. 012569) to generate $Sim1^{Cre/+}$;$Rosa26^{floxstopTdTom/+}$/$^{Gt(Rosa)26floxstopH134R/EYFP/+}$ (Sim1TdTom/Ai32 or Sim1TdTom/ChR2). *In vitro* optogenetic electrophysiological experiments were performed in 23 neonatal (P1-P16) Sim1TdTom/ChR2 mice of both sexes.

BDA and CTB injections

Recovery surgery protocol for antero- and retrograde dye injections. 9 adult mice of both sexes were subjected to spinal injection of BDA at spinal segments L2, L3 or L4/L5 for anterograde or CTB-A488 at spinal level T8 for retrograde tracing. Once animals were in a deep surgical plane and under aseptic conditions, skin overlying the vertebrae of interest was opened

with a scalpel, and back muscles blunt dissected to reveal the posterior spinous processes. Forceps were used to perform a single vertebrae laminectomy to expose the spinal cord and dura was opened with a 27-gauge needle. Injection of 1 µL of 1% biotin dextran amine (BDA-10,000 mW, Thermo Fisher Scientific Cat# D1956, RRID: AB_2307337) or cholera toxin B Alexa 488 (CTB-A488, Molecular Probes, Cat # C34775). BDA was injected near the left midline using a stereotaxic micromanipulator and 700-900 µm into the spinal cord. Injection was delivered using a motorized pico-injector with a 75RN SYR 5 µl Hamilton syringe fitted with a single-barrel borosilicate capillary glass (A-M Systems INC.) pulled to a ~120 µm tip. The dye was injected over a 5-minute period, the needle remained in place for an additional 10 minutes to prevent backdraw into the pipette. Each animal received slow-release buprenorphine (0.5 mg/kg) and glucose solution (0.02 ml/g), returned to a heated cage for 2 hours until fully functional and then were returned to home-cage and health was monitored daily. 7 days later, animals were terminally perfused as described in "Immunohistochemistry and Imaging" and processed as follows.

Immunohistochemistry and Imaging

Immunohistochemistry protocol. Under inhalant isoflurane anesthesia, adult Sim1TdTom mice were transcardially perfused with 4% PFA in phosphate-buffered saline (PBS). Spinal cords were dissected free and placed in 4% PFA overnight, and subsequently cryoprotected in 30% sucrose. For sectioning, the thoracic spinal cord was divided into two approximately equivalent-sized portions, with the rostral portion containing ~T1 – T6/7 and the caudal portion ~T7 – T13. Lumbar portions were sectioned in one contiguous section at 30 µm. Thoracic spinal cord was sectioned at 18 µm (BDA-injected mice) and 30 µm (all other mice) using a cryostat and mounted on glass slides for immunohistochemistry. To characterize V3 neuron somas

throughout thoracic and lumbar segments, images were obtained on a Zeiss Axioscope 40 and every third section (~ every 450 µm) per slide was examined and/or counted (n = 5 mice). To characterize V3 terminals, SPNs and VGluT2 expression in the thoracic spinal cord, every fifth section (rostro-caudal distance of ~90 µm between sections) was processed for immunohistochemical visualization of TdTomato and ChAT and VGluT2, with the remainder preserved for other purposes. For BDA-injected mice, every fifth section was examined, representing inter-section distances of ~ 90 µm. All sections were washed three times for 10 minutes each in 0.2% PBS-T, followed by 10-minute antigen retrieval (55 °C incubation in Tris-EDTA buffer) and an additional three washes in 0.2% PBS-T for 10 minutes each. 10% normal donkey serum block in 0.2% PBS-T was applied for one hour. Sections were then incubated with primary goat anti-dsRED (1:1000, Takara Bio, Cat# 632496, RRID: AB_10013483), goat anti-ChAT (1:400, Millipore, Cat# AB114P, RRID: AB_2313845) and guinea-pig anti-VGluT2 (1:500, Millipore, Cat# AB2251-I, RRID: AB_2665454) for 72 hours at 4 °C. Sections were then washed three times for 10 minutes each in 0.2% PBS-T followed by incubation with appropriate secondary antibodies conjugated to Alexa 488, Cy3 and Alexa 647 (1:500; Molecular Probes, Cat# A-11055, RRID:AB_2534102; Jackson Immuno Research Labs, Cat# 711-165-152, RRID:AB_2307443; Jackson Immuno Research Labs, Cat# 706-605-148, RRID:AB_2340476, respectively) for two hours. Sections were then washed one time for 10 minutes in 0.2% PBS-T followed by two washes for 10 minutes each in Tris-HCL 50 mM, then dried, mounted in Vectashield hardset mounting medium (Vector Laboratories) and cover slipped. For mice injected with BDA, sections were processed as described but immunolabelling for VGluT2 was removed and the secondary antibody Streptavidin647 (1:500, Thermo Fisher Scientific, Cat# S-21374, RRID: AB_2336066) was used at the appropriate step to label for BDA. Similarly, in a

subset of mice that received thoracic injections of CTB, lumbar spinal cords were washed, mounted in Vectashield hardset mounting medium and cover slipped.

Image Analysis. Sections confirming BDA and CTB injection sites and CTB positive lumbar V3 INs were imaged using a Zeiss Axio Imager Z.2 upright microscope. BDA injection sites were reconstructed using tiled images obtained under 10x magnification within Zen Blue software (Version 3.5). Images were used to confirm injection site and determine rostro-caudal and transverse distribution of injected dye. For CTB-injected mice, CTB-A488^{+}/tdTomato^{+} somas in lumbar cord were counted by creating tiled, Z-stack images (7 – 10 z-stacks, range of 6 µm – 9 µm) at 10x magnification and counted in ZenLite software (Version 3.6). For each animal, 9 – 10 sections were imaged and analyzed throughout the entire lumbar spinal cord per animal (L1 – L6; n=4 animals). To correspond with previous anatomical observations of three distinct V3 sub-populations (Borowska et al., 2013), tiled images of each transverse spinal cord section were divided into dorsal, intermediate and ventral regions for both sides of the lumbar spinal cord to compare double labelled somas ipsi- and contra-lateral to the injection site. For a neuron to be classified as a V3 IN labelled with CTB, either a distinguishable overlap of the neuron's soma with CTB fluorescence was present or the neuronal soma had to have perinuclear labelling with 4-5 distinct vesicle speckles within demarcations of the soma[i] {Conte, 2009 #1064}

A Zeiss Airyscan LSM 880 confocal microscope was used to image VGluT2/TdTom^{+} or BDA/TdTom^{+} neuronal processes apposing SPNs (ChAT^{+} neurons) in thoracic IML. For each rostral (~T1 – T6/7) and caudal (~T6/7 – T13) segment, 14 – 20 ROIs containing the IML were selected with at least 90 µm of inter-section length intervals to obtain a representative rostro-caudal distribution of IML regions and SPNs per mouse (n=4). Each IML region was imaged

using 7 – 14 vertical planes [7 – 14 Z-stacks per image, 3.6 – 12.8 µm range] at 63x magnification. Laser settings were optimized and replicated within each animal, for consistency between images. Left and right IML SPNs were selected and imaged based on visibility of at least one SPN soma per ROI. Z-stack images were then imported into IMARIS software for 3D reconstruction and quantitative analysis using the "Surface" tool. Synaptic boutons (VGluT2) less than 1 µm from SPN somas were quantified and considered doubled labelled if there was overlap with $TdTom^{+}$ surfaces. Similar, doubled labelled contacts of BDA/$TdTom^{+}$ were considered as synaptic boutons when less than 1 µm from SPN soma. To examine presumed V3 IN terminal density in thoracic IML, the right half of thoracic grey matter was tiled imaged using a 20x objective lens on the Zeiss Airyscan LSM 880 confocal microscope, taking 2 – 3 Z-stacked (2.494 – 4.987 µm range) images per segment (12 images per mouse to correspond to roughly each spinal segment, n = 3 mice). Images were then reconstructed and analyzed in IMARIS. "Spots" detection method was used to filter and select presumed V3 IN terminals. Cell bodies and long neuron processes were excluded from quantification in IMARIS using its size and shape exclusion and re-iterative learning features. A region of interest set in IMARIS around the IML (278 x 277 µm) was used to analyze and quantify V3 neuron synaptic terminal density for each segment. Individual X–Y coordinates for each synaptic terminal were exported to Excel and GraphPad Prism for subsequent analysis. XY coordinates for each synaptic terminal were also exported and transformed into contour plots using RAWGraphs (https:app.rawgraphs.io).

Electrophysiology

Spinal cord slice preparations. Experiments were performed on spinal sections isolated from 23 neonatal (P1-P16) $Sim1^{Cre/+}$;$Rosa26^{floxstopTdTom/+}$/Gt(Rosa)$26^{floxstopH134R/EYFP/+}$ (referred to as Sim1TdTom/ChR2) mice. Isolation and preparation of sections, and electrophysiological

recording methods have been previously described (Chopek et al., 2018b). Briefly, animals were anaesthetized with isoflurane, decapitated at the medulla-spinal cord junction and spinal cords dissected out in ice-cold dissecting artificial cerebrospinal fluid aCSF, composed of (mM): KCL 3.5, NaHCO3 35, KH2PO4 1.2, MgSO4 1.3, CaCl2 1.2, glucose 10, sucrose 212.5, MgCl2 2.2, pH equilibrated to pH 7.4 with 95% 0_2 & 5% $C0_2$. Once dissected free, thoracic spinal cords were immediately secured in agarose and sectioned at 350 µm using a vibratome (Leica VT1200S, Leica) and then incubated in warm (30 ^{0}C) aCSF for a minimum of 30 minutes before performing electrophysiological experiments. Incubation and recording ACSF was composed of (mM): NaCl 111.0, KCl 3.085, D-glucose 10.99, $NaHCO_3$ 25.0, $MgSO_4.7H_2O$, $CaCl_2$ 2.52, KH_2PO_4 1.1, equilibrated to pH 7.4 with 95% O_2 & 5% CO_2.

Intact spinal cord preparations. Spinal cords were dissected free from Sim1TdTom/ChR2 mice as described above in 'Slice preparations' but remained intact with dorsal and ventral roots attached. Once free, connective tissue was carefully removed from spinal cord tissue and secured ventral side up with fine insect pins. To retrogradely label SPNs, rhodamine dextran amine dye (RDA) was applied to cut T6-T8 ventral roots on one or both sides of the spinal cord using glass suction pipettes with internal diameters of 100-120 µm. Ventral roots were cut close to their exit from the spinal cord to minimize labeling time. Retrograde labeling of thoracic SPNs continued in the dark at room temperature for at least 3 hours (Szokol et al., 2008). A block of agar was prepared in advance with one side of the block cut with a scalpel to provide a 30-degree incline. The spinal cord was then mounted on the agar block and the corresponding labeled thoracic spinal segment attached to the angled surface of the agar block with acrylic glue. The spinal cord at the level of the agar block was then sectioned with a vibratome. A portion of the spinal cord was then glued to a sylgard-coated (Sylgard, Dow

Corning, MI, USA) recording chamber designed and 3D printed in-house specifically for these experiments. In particular, the obliquely cut surface of the spinal cord was placed on a sylgard 'ramp' to enable visualisation and patch-clamp recordings of SPNs under fluorescence while preserving and maintaining continuity with the lumbar spinal region for optical stimulation.

Whole cell patch-clamp recordings and optogenetic stimulation. Slices or spinal cord preparations were transferred to a recording chamber mounted on a Zeiss AxioExaminer microscope and perfused with oxygenated room-temperature aCSF. Cells were visualized using a 20x wide aperture (1.2 nA) water-immersion objective lens, a CCD camera (CoolSNAP EX OCD Camera, Photometrics, AZ) and Slidebook 6.0 software (Intelligent Imaging Innovations, CO, USA, RRID:SCR_014300). Patch pipettes were pulled with a Sutter puller (source Brian J Schmidt) and those with 4-6 MΩ resistances were filled with the following (mM): K-gluconate, 128; NaCl, 4; $CaCl_2$, 0.0001; Hepes, 10mM, glucose, 1mM; Mg-ATP, 5; and GTP-Li, 0.3. Whole cell patch-clamp recordings were made under current-clamp Multiclamp 700B amplifier (Molecular Devices, California, USA, RRID: SCR_014300). Recordings were low pass filtered at10 kHz and acquired at 25 kHz with CED Power 1401 AD board and displayed and recorded using Signal software (Cambridge Electronic Design, Cambridge UK). Before performing an optical stimulation protocol, rheobase (defined as the minimum current to elicit a single AP was collected to determine cell excitability). Before the optical stimulation protocol, we recorded rheobase and repetitive firing in response to 1 second depolarizing current steps from each SPNs. In slice preparations, presumed SPNs (small neurons visualized in the IML, with TdTom fluorescence noted near the soma) were patched and responses recorded. Using a spatial light modulator system as previously described (Chopek et al., 2018b; Chopek et al., 2021), a region of interest slightly greater than the SPN soma was created for optical stimulation of presumed V3

terminals apposing the patched SPN. Blue light was delivered in five 500ms pulses at 5 Hz at a laser power of ~2.5 mW. For whole cord preparations with thoracic surface exposed, SPNs that were retrogradely labelled with RDA were patched and responses recorded. A region of interest covering the ventral L2 segment was created for optical stimulation of presumed ventral L2 V3 neurons and likely axons of passage of caudal lumbar segments. Blue light was delivered in five 500ms pulses at 5 Hz at a laser power of ~2.5 mW. In a subset of slice experiments, lumbar V3 neurons were patched and optically activated to confirm that optical stimulation resulted in AP generation in V3 neurons.

Statistics

Statistical Analysis. Data are presented as mean ± SD. As is common for discovery experiments, no statistical method to predetermine sample size and no randomization or blinding procedures were used. Statistical analyses were done using GraphPad Prism (V9.5 for MacOS, GraphPad Software, San Diego, California USA, www.graphpad.com) to analyze quantification of V3 cell bodies, presumed V3 terminals and anterograde and retrograde injection data. One-way ANOVA and Tukey's multiple comparisons tests were performed. Statistical significance was set to $p < 0.05$.

RESULTS

V3 IN cell bodies located throughout the thoracic spinal cord.

V3 INs cell bodies have been localized within caudal thoracic and upper lumbar spinal regions (Borowska et al., 2013) and electrophysiological evidence suggests a role for V3 INs in lumbar locomotor activity (reviewed by (Ziskind-Conhaim and Hochman, 2017), but their presence or function(s) in more rostral thoracic regions has not been investigated. Thus, we

examined the anatomical distribution of V3 cell bodies throughout the thoracic and lumbar spinal cord. Our findings regarding V3 soma in lumbar regions were consistent with previous reports, with three subpopulations (dorsal, ventral and intermediate subpopulations) in the rostral lumbar and two populations (intermediate and ventral) observed in caudal lumbar regions (e.g., Fig. 1C).

In the thoracic spinal cord, we observed V3 soma throughout T1-T13 at similar transverse locations as observed in lumbar regions (Fig. 1). V3 soma were not observed within thoracic IML regions. V3 soma in the thoracic region were smaller and less densely distributed compared to V3 cell bodies located in the lumbar region (Compare panels in Fig. 1C – and graph in 1B). On average (n=4), similar numbers of V3 cell bodies were observed per 30 µm section in rostral versus caudal thoracic segments (16.6 ± 5.94 V3 soma in T1-T6; 14.0 ± 5.36 V3 in T7-T13; Fig. 1B & Fig. 1C a-c vs Fig. 1C d-f). The highest number of V3 somas were observed in lumbar sections (i.e., L1 – L3 with 32.85 ± 8.14 and L4 – L6 with 32.05 ± 4.59 V3 neurons per section, $p < 0.0001$; Fig. 1B & Fig. 1C g-i vs Fig.1C j-l). In addition to V3 cell bodies, V3 $TdTom^+$ fibres were observed throughout the thoracic spinal cord and within IML regions.

We therefore characterized the distribution of presumed V3 synaptic terminals within the rostro-causal thoracic grey matter generally and with a particular focus and analysis of terminals within the IML. To do so we identified $TdTom^+$ presumed nerve terminals (1 section every ~ 900 µm) throughout the thoracic spinal cord, including a pre-defined IML region in Rexed lamina VII (12 sections per animal, n = 3). V3 terminals were identified at all rostro-caudal levels of the thoracic region, within the dorsal and ventral horns, with an expected high density in lamina IX, close to the somatic motor nuclei (e.g., ~T10 in Fig. 2B). For consistency, a pre-defined area (278 µm x 277 µm) of the IML was selected for quantifying the number of V3 terminals for each section (Schematic in Fig. 2A, blue box). Each presumed $TdTom^+$ terminal was marked with an

XY coordinate and exported from IMARIS to develop contour plots (heat maps) of the relative distribution of terminals throughout grey matter (see representative example of Fig.2A transformed to Fig.2B). Numbers of terminals within the grey matter ranged from ~2500 – ~17700 (mean = 9646, 7577, 5526 for mouse 1, 2 and 3 respectively) and within the IML, terminal numbers ranged from ~500 – ~2400 per section (mean= 1279, 1166, 875 for mouse 1, 2 and 3 respectfully), depending on the rostrocaudal level of the section. In particular, there were higher numbers of terminals in the pre-defined IML region in rostral (~ ≥ 1,000) compared to caudal (~ ≤ 1,000) thoracic SC (Compare heat maps of T1 to T12/13 in Fig. 2B and numbers in Fig. 2C) with highest numbers observed between ~T4 and T6 (Fig. 2C).

Together these results demonstrate that V3 cell bodies are located throughout the thoracic spinal cord, located in similar populations, but at approximately half the size and number observed in lumbar regions. These results also demonstrate that there is a proportionally large quantity of V3 neuronal terminals within the IML region of the thoracic spinal cord (presumed V3 IML puncta account for 14.3%, 15.9% and 21.2% of all puncta within grey matter of one side of spinal cord for animal 1, 2 and 3 respectively).

20% of glutamatergic input apposing thoracic SPNs arises from V3 interneurons

As only VGluT2$^+$ terminals are found apposing SPNs (Llewellyn-Smith et al., 1992; Llewellyn-Smith et al., 2007), VGluT2$^+$ terminals likely account for all glutamatergic inputs to SPNs. In order to determine whether any of the excitatory V3 terminals observed within the thoracic IML directly apposed SPNs, we examined our sections labelled with ChAT (SPNs), VGluT2 and DsRed. Confocal z-stack images from rostral (Figure 3A) and caudal thoracic regions (Figure 3C) were imported into IMARIS software for 3D reconstruction. Using the 3D reconstructions, the number of VGluT2$^+$ and double-labelled VGluT2$^+$/DsRed$^+$ synaptic

terminals apposing SPNs were calculated and plotted for rostral and caudal thoracic regions for each animal (Fig. 3E). A total of 56-80 SPN sections were reconstructed and analyzed for each rostral and caudal thoracic region per mouse (n=4). On average, 107.2 VGluT2$^+$ contacts apposed each SPN (range: 0 – 645 VGluT2$^+$ contacts). Over all sections examined for each animal, 16.9% – 26.6% (n=4 mice) of VGluT2$^+$ synaptic terminals were double labelled with DsRed, indicating that these terminals arose from V3 neurons (Fig. 3A & C). Similar proportions of excitatory V3 synaptic terminals were observed apposing SPNs within rostral versus caudal thoracic regions within each animal (Fig. 3E; $p = 0.43$, n =4). We noted that SPN size varied throughout the thoracic spinal cord, therefore we examined the ratio between number of V3 terminals apposing each SPN normalized to SPN surface area and found a similar ratio between high (0.63+/-) and low (0.64+/-) thoracic SPNs indicating no difference in the number of V3 terminals apposing high or low thoracic SPNs ($p = 0.98$).

In order to determine if any of the V3 synaptic terminals apposing thoracic SPNs originated from lumbar V3 neurons, we performed experiments in which BDA was injected in various lumbar segments. We then quantified the proportion of V3 contacts (DsRed$^+$) that were also BDA$^+$ and apposing ChAT$^+$ SPNs. Four animals contributed to this series (2 injected at L2, 1 at L3 and 1 at L4/L5). A typical example is shown in Figure 3 with images taken from the rostral (Fig. 3A & 3B) and caudal (Fig. 3C & 3D) thoracic regions demonstrating that a portion of the V3 synaptic input onto SPNs originates from V3 neurons in the lumbar region. Overall, 3.8 % – 21.9% of total V3 contacts (DsRed$^+$) were also BDA$^+$, demonstrating that lumbar V3 neurons provide ascending synaptic input onto thoracic SPNs, and double-labelled terminals were observed when injected at either L2, L3 or L4/5 (Fig. 3E).

In this series we also compared the proportion of BDA^+ and $DsRed^+$ presumed terminals in rostral versus caudal thoracic regions to determine if there was any evidence to suggest a somatotopic organization to the ascending input onto thoracic SPNs from lumbar V3 neurons. Thus, we compared the proportion of double-labelled terminals observed in rostral (T1-T6; Fig. 3B) versus caudal (T7-13; Fig. 3D) thoracic regions for BDA injections at rostral lumbar (L2, Fig. 3E) versus caudal lumbar (L4/5; Fig. 3E) sites. Figure 3E demonstrates that there were a greater proportion of BDA^+ and $DsRed^+$ terminals in rostral thoracic versus caudal thoracic regions for animals injected with BDA at rostral lumbar sites (13.9% vs 6.4% respectively, and visually from Fig. 3B & 3D, n = 2 mice, * $p < 0.0265$). Conversely, animals injected with BDA at caudal lumbar sites demonstrated a greater proportion of BDA^+ and $DsRed^+$ terminals in caudal compared to rostral thoracic regions (22.0% vs 8.5% respectively, Fig. 3E, n = 1 mouse, ** $p < 0.0019$). In contrast, a similar proportion of BDA^+ and $DsRed^+$ terminals were observed rostral and caudal regions in animals with BDA injection at the mid-lumbar (L3) level (6.95 % vs 9.23% respectively, Fig. 3E, n = 1 mouse, $p < 0.977$). These findings suggest that ascending input from lumbar V3 neurons may be somatotopically arranged, as opposed to a pattern of ascending input throughout the entire thoracic region, regardless of lumbar V3 segmental location.

We next thought to determine which V3 subpopulations innervate thoracic SPNs. To achieve this, we unilaterally injected CTB at the T8 segment and counted CTB^+ V3 INs throughout the lumbar spinal cord (Fig. 4, n = 3). Due to the difficulty in precisely targeting SPNs, which is located near white matter that may have V3 axons of passage, we examined injection site for potential spread and present descriptive evidence from injections and compared to the one successful injection (Fig. 4B) in which no CTB was evident in the white matter. We

found widespread CTB uptake in the dorsal, intermediate and ventral V3 populations both ipsilateral and contralateral to injection site (Fig. 4C & D). A similar percentage was seen between the confirmed ipsilateral grey matter injection and the three other injections with ipsilateral dorsal (73.5% and 73.8%), intermediate (62.7% and 53.3%) and ventral (59.7% and 58.0%) lumbar V3 INs positive with CTB. Similar values we had seen on the contralateral side with dorsal (64.3% and 70.0%), intermediate (55.1% and 53.5%) and ventral (67.4% and 66.9%) positive with CTB (Fig. 4E). This suggests that, both contralateral and ipsilateral and dorsal and ventral lumbar V3 INs project near thoracic IML, consistent with previous findings of both ipsilateral and contralateral projections (Zhang et al., 2008; Borowska et al., 2013; Blacklaws et al., 2015; Chopek et al., 2018b)

Spinal V2a and V0 neurons do not appose SPNs

As part of our investigations to identify potential sources of intraspinal locomotor-related neuronal input onto sympathetic-related neural circuitry, we also performed anatomical experiments to determine whether two other genetically defined candidate spinal neuron populations provide synaptic input to thoracic SPNs or the IML region generally. Thus, the first population we examined were the local projecting, glutamatergic neurons V2a neurons involved in left-right coordination and defined by the transcription factor Chx10 (Al-Mosawie et al., 2007; Lundfald et al., 2007; Crone et al., 2008; Crone et al., 2009). Examined in 2 Chx10:eGFP mice, we observed VGluT2^{+}/GFP^{+} fibres within the IML but did not observe any double-labelled (VGluT2^{+}/GFP^{+}) terminal apposing thoracic SPNs. In these same animals, we did observe VGluT2^{+}/GFP^{+} terminals apposing lumbar motoneurons, suggesting that our negative findings regarding thoracic SPNs was not due to a weak fluorescent signal or lack of GFP expression in terminals of Chx10 mice.

In another series of experiments, we examined whether the V0 neuron population provides synaptic input onto SPNs. V0 neurons can be subdivided into 3 subpopulations ($V0_c$, $V0_D$, $V0_v$) each with a different neurotransmitter, projection pattern and role in locomotion (Moran-Rivard et al., 2001; Pierani et al., 2001; Lanuza et al., 2004; Zagoraiou et al., 2009; Talpalar et al., 2013). Thus, we examined in 2 Dbx1Cre:tdTomato mice, in which all three populations are visualized with red fluorescent protein, we did not see any presumed $TdTom^+$ terminals apposing thoracic SPNs. Similar to our observations for the V2a population noted above, we did observe terminals apposing lumbar motoneurons, suggesting that our negative findings regarding thoracic SPNs for the V0 population were not due to a weak fluorescent signal or lack of TdTomato expression in terminals of Dbx1 mice.

Lumbar and thoracic V3 neurons provide functional excitation to thoracic SPNs

Based on our anatomical demonstration that V3 spinal neurons provide direct synaptic input to thoracic SPNs, we performed a series of electrophysiological experiments to determine if activation of V3 neurons can excite SPNs. First, we used immunohistochemical microscopic examination to confirm Channel rhodopsin expression in V3 neurons in $Sim1^{Cre/+}$;$Rosa26^{floxstopTdTom/+}$/$Gt(Rosa)26^{floxstopH134R/EYFP/+}$ mice (Fig. 5A) and that $TdTom^+$/$Chr2^+$ terminals were present in thoracic IML regions (Fig 5B). We then confirmed that we could elicit action potentials (APs) in lumbar V3 neurons in response to optical stimulation (Fig. 5C, n=10). In 10 out of 10 V3 neurons tested, optical stimulation over the soma of the patched V3 elicited repetitive firing of the neuron.

Next, we determined whether optical stimulation of V3 neuron terminals in thoracic slice preparations could excite putative SPNs in the IML. Examined in 10 presumed SPNs optical stimulation (480 nm wavelength) of V3 terminals directly over the patched presumed SPN using

a focal light source from a spatial light modulator elicited excitatory post synaptic potentials (EPSPs, Fig. 6A n=2), action potentials (Fig. 6B n=4) or no response (n=4). Presumed SPNs in slice recording had an average rheobase value 20 ± 5 pA.

In our final electrophysiological series of experiments, we determined whether optical stimulation of lumbar V3 neurons could excite thoracic SPNs located multiple segments rostral to the stimulation site. As noted in Methods, we targeted SPNs in T6-T8 and used the whole-cord preparation with an obliquely cut surface with a targeted caudal edge at T8. Retrograde labelled SPNs were visualized and patched (n=20). Optical stimulation over the ventral surface of the ventral L1-L2 spinal cord elicited EPSPs (n=4), APs (n=5), or failed to elicit a response (n=11) in thoracic SPNs (Fig. 7). Backfilled SPNs had a similar rheobase value 25 ± 10 pA as the presumed SPNs recorded in slice. Interestingly from both slice and whole cord recordings, SPNs that generated only a single AP in response to 1 second depolarizing current injection only 1 of 15 generated an excitatory responded to optical stimulation while the 14 remaining SPNs did not respond to optical stimulation. Whereas, in the 15 SPNs that fired repetitively during the 1 second current injection, an excitatory response was evoked in 14 of the 15 SPNs.

Taken together, these anatomical and electrophysiological experiments provide strong evidence for an ascending intraspinal excitatory neuronal projection from lumbar locomotor-related V3 neurons to thoracic sympathetic preganglionic neurons.

DISCUSSION

Here, we demonstrate that locomotor related V3 INs project to and excite SPNs throughout the entire thoracic spinal cord and account for ~20% of glutamatergic input to SPNs. We further demonstrate strong ascending input from lumbar V3 INs to thoracic SPNs, and that when optically stimulated, evokes post synaptic responses in SPNs. That is, we demonstrated an

intraspinal connection between lumbar V3 INs and thoracic SPNs. We hypothesize that this intraspinal connection allows for the spinal cord the capability to integrate locomotor and sympathetic function, to ensure appropriate metabolic and homeostatic support during movement and exercise.

At the supraspinal level, clear evidence demonstrates the brainstem is capable of coordinating and integrating circuitry for movement and sympathetic function. Stimulation of the mesencephalic locomotor region (MLR) or subthalamic locomotor region not only results in locomotion but also an increase in respiratory function (Eldridge et al., 1981) and cardiovascular responses, in an activity and intensity dependent manner (Bedford et al., 1992). Both of these increased sympathetic responses persisted when neuromuscular blockers were applied suggesting a central source regulating both locomotor and autonomic functions (Chong and Bedford, 1997). Confirming that these responses are mediated by a central source, two direct pathways from the MLR were recently found, one pathway projecting to glutamatergic neurons in the medulla to initiate movement, and one projecting to the cardio-respiratory centre located in the rostral ventral lateral medulla (Koba et al., 2022).

Further evidence for brainstem control of locomotor and autonomic was demonstrated when glutamatergic Chx10 neurons located in the gigantocellular nucleus of the medulla and involved in locomotion (Bretzner and Brownstone, 2013; Bouvier et al., 2015; Schwenkgrub et al., 2020; Usseglio et al., 2020) are ablated, respiration rate generated in the nearby pre-Botzinger complex is reduced (Crone et al., 2012). Similar, MLR stimulation results in increased blood pressure, heart rate and vasoconstriction prior to any rhythmic motor activity, even in the absence of movement in the unanesthetized, decerebrate paralyzed rat (Bedford et al., 1992; Chong and Bedford, 1997; Koba et al., 2005). Studies using pseudorabies virus demonstrated higher-order

neurons that function in both somato-motor and sympathetic function termed somato-motor-sympathetic neurons (Kerman et al., 2003; Kerman et al., 2006; Kerman et al., 2007; Kerman, 2008). These findings suggest that communication and adequate activity in both brainstem autonomic and locomotor centres is required for movement to occur. We propose a similar role within the spinal cord, in which V3 INs are involved in integrating and communicating with both autonomic SPNs and lumbar locomotor networks.

A conceptual framework put forth the idea that the spinal cord is also capable of integrating motor and sympathetic function, which likely becomes critically important after SCI, when descending commands are removed (Cowley, 2018). A recent scoping review supports this concept, as epidural stimulation used to improve motor function after SCI also improved at least one autonomic function (Flett et al., 2022a). We hypothesized the mechanisms mediating improved locomotor and autonomic function involves ascending propriospinal neural networks. Ascending propriospinal neurons arising from the lumbar spinal cord can coordinate and entrain the locomotor rhythm on both thoracic respiratory neurons (Le Gal et al., 2016) and the cervical CPG network (Juvin et al., 2012; Zhang et al., 2022). Although we examined multiple glutamatergic neurons, including several that are classified as propriospinal, our results indicate that V3 INs may be the major source of spinal glutamatergic input to SPNs. V3 INs are ideal candidates to communicate and integrate locomotor and sympathetic functions as they have long ascending projections from lumbar to cervical spinal cord, and are involved in stability of locomotion and coordination between left and right hindlimbs and between hindlimbs and forelimbs (Zhang et al., 2008; Blacklaws et al., 2015; Danner et al., 2019; Zhang et al., 2022).

We demonstrated that ~20% of all VGluT2^{+} synaptic contacts on SPNs arise from V3 INs. As SPNs only receive input from glutamatergic neurons that use glutamatergic transporter VGluT2

(Llewellyn-Smith et al., 2007), this indicates that 20% of glutamatergic inputs to SPNs are from V3 INs. Although it is known that SPNs receive intraspinal input including glutamate, GABA, and acetylcholine, little is known of the identity of those neurons providing input arise from (Llewellyn-Smith, 2009). However, it likely involves neurons located in laminae V, VII and X and involves input from locally projecting spinal interneurons (Llewellyn-Smith, 2009). In our preliminary investigations, we did not see any input from local projecting $Chx10^{+}$ spinal INs or from DBX^{+} spinal INs apposing SPNs. Thus, 20% of glutamatergic input to SPNs represents a large source of spinal excitatory input and indicated that V3 INs likely provide the majority of excitatory spinal input to SPNs. We conjecture the remaining excitatory inputs to SPNs are from brainstem centres including the rostral ventral lateral medulla.

Various synaptic inputs to SPNs demonstrate rostro-caudal differences or segments with high or low inputs to SPN. For instance, the greatest density of nerve terminals and fibres in the IML arising from Enkephalin expressing neurons was in T1-T8. For substance P expressing neurons the greatest density was between C8-T12 and T11-L1, and for serotonergic neurons was T1-T5 in cat (Krukoff et al., 1985). A similar distribution of serotonergic fibres within the IML was also seen in the rabbit, with the greatest density in T3-T6 and L3-L4 and minimal numbers T1 and T10-T12 (Jensen et al., 1995). This differential rostro-caudal input to SPNs, permits specific functional groups of SPNs to respond in different ways to the same homeostatic challenge. Furthermore, innervation of target tissues demonstrates a topographical organization from SPNs. Rostral thoracic SPNs via Superior Cervical Ganglia and Stellate Ganglion are involved in the regulation of upper body targets such as pupils, salivary glands and heart. SPNs in mid thoracic spinal cord via Celiac ganglion control mesenteric vasculature, gut motility and

secretion and adrenal medulla. SPNs in the caudal SPN aid in regulation of lower body organs such as urinary bladder and reproductive organs.

We found a peak density of V3 IN contacts within T4-T7 segments, which via post-sympathetic neurons innervate the heart and adrenal medulla. In addition, we also demonstrated that V3 INs innervate thoracic somatic MNs. Taken together, it is conceivable that in response to increased motor function, lumbar V3 INs provide additional excitation to SPNs to increase heart rate and stroke volume, release circulating catecholamines and to thoracic MNs for increased demands of respiration and posture. In addition, one would expect less innervation of SPNs involved in regulating gut motility or reproductive organs as these are not vital for sustained movements or exercise. That is, there is likely a selective innervation of SPNs from neurons involved in locomotion, to ensure adequate organ and tissue support for movements.

Overall, this is the first demonstration of an anatomical and functional connectivity between neurons involved in locomotion with neurons involved in sympathetic functions. We propose that similar to the brainstem, communication between locomotor and autonomic centres occurs within the spinal cord. This communication occurs from long projecting ascending V3 propriospinal neurons ensuring that adequate metabolic and homeostatic support occurs during sustained rhythmic activity such as exercise. And that these neurons may be of therapeutic importance for improving autonomic and motor function after SCI.

ACKNOWLEDGEMENTS

We thank Shannon Deschamps for assistance with surgical and post-operative animal care and assistance with immunohistochemistry.

GRANTS

This work was supported by the University of Manitoba, Rady Faculty of Health Sciences, Research Manitoba, NSERC (RGPIN-2015-04810), Canada Research Chairs and the Craig H. Neilsen Foundation.

DISCLOSURES

No conflicts of interest, financial or otherwise, are declared by the authors.

AUTHOR CONTRIBUTIONS

KCC & JWC conceived the research project; CC, KCC & JWC conceived and designed experiments; CC, CVN, NS & JWC performed experiments; CC & NS analyzed data; CC, KCC & JWC interpreted results; CC, JWC prepared figures; CC, CVN, JWC and KCC drafted the manuscript; and JWC & KCC edited and revised manuscript. All authors approved the final version of the manuscript.

LEGENDS

Abstract Figure. V3 locomotor-related neurons provide anatomical and functional input onto autonomic sympathetic neurons. A) Neuroanatomical tracing and immunohistochemistry methods schematic. B) Schematic methodology of electrophysiology protocols. C) Summary of results demonstrating that lumbar V3 interneurons provide ascending glutamatergic connections

onto autonomic sympathetic neurons situated in the intermediate lamina (IML) of the thoracic spinal cord.

Figure 1. V3 neuronal cell bodies distributed throughout the thoracic and lumbar spinal regions. A) Schematic demonstrating Rexed Laminae and regions represented in panel C-b,e,h,k (dorsal section, outlined in turquoise colour) and C-c,f,i,l (ventral section, outlined in fuchsia colour). C) Summarizes mean numbers (+/- S.D.) of cell bodies counted per section for each region. No differences in V3 cell bodies were seen between thoracic segments and between lumbar segments but significant difference was seen between thoracic and lumbar segments ($P < 0.0001$, n=4)

Figure 2. Presumed V3 glutamatergic neuron terminals observed within the IML at all thoracic spinal segments, with highest density observed in mid-thoracic spinal levels. A) Schematic demonstrating organization of V3 terminals found in grey matter of spinal cord. XY coordinates of V3 terminals were exported to create contour maps. B) Contour plots of relative V3 terminal density from XY coordinates exported from IMARIS from one adult mouse in grey matter of thoracic spinal cord. Note the high density of V3 terminals in both the IML and grey matter. C) Graph summarizing numbers of terminals observed in IML ROI (278 µm x 277 µm) at each thoracic spinal level for each animal examined (n=3 animals, 12 sections per animal). Numbers of terminals within the grey matter ranged from ~2500 – ~17700, and within the IML, terminal numbers ranged from (~500 – ~2400) per section, depending on the rostrocaudal level of the section.

Figure 3. Injection of BDA neuronal tracer into lumbar spinal cord reveals ascending synaptic input from V3 neurons located in the lumbar region. A) Double labelled VGluT2 and TdTom terminals apposing SPNs in rostral thoracic spinal cord. Double labelled neurons

indicated with arrowheads. B) Double labelled BDA and TdTom terminals apposing SPNs in rostral thoracic spinal cord. Double labelled neurons indicated with arrowheads. C) Double labelled VGluT2 and TdTom terminals apposing SPNs in caudal thoracic spinal cord. Double labelled neurons indicated with arrowheads. D) Double labelled BDA and TdTom terminals apposing SPNs in caudal thoracic spinal cord. Double labelled neurons indicated with arrowheads. **Scale** = 20 μm for panels (A-D). E) Rostrocaudal distribution of percentage of double labelled VGluT2^{+}/TdTom^{+} and BDA^{+}/TdTom^{+} puncta throughout the thoracic spinal cord. Glutamatergic excitatory V3 IN innervation on SPNs was ~20% with no significant difference between T1-T6 and T7-T13 segments ($p = 0.43$, Brown-Forsythe test, $n = 4$ mice). L2 BDA injections demonstrated a higher percentage of BDA^{+}/TdTom^{+} terminals in rostral thoracic segments compared to caudal thoracic segments (* $p < 0.0265$, $n = 2$ mice). In contrast, L4/L5 BDA injections demonstrated a higher percentage of BDA^{+}/TdTom^{+} terminals in caudal thoracic segments compared to rostral thoracic segments (** $p < 0.0019$). L3 BDA injections showed no significant difference in percentage of BDA^{+}/TdTom^{+} terminals in rostral thoracic versus caudal thoracic segments ($p < 0.977$).

Figure 4. Injection of CTB neuronal tracer into thoracic segment T8 reveals subpopulations of lumbar V3 neurons projecting to thoracic spinal cord. A) Schematic of lumbar spinal cord section. Sections were divided into dorsal, intermediate and ventral regions on left (L) and right (R) sides of the spinal cord and counted based on these regions of interest. B) Reconstructed T8 injection site. CTBA488 was injected unilaterally into the spinal cord. This injection was confined to the grey matter of the right-side spinal cord. **Scale** = 500 μm. C) L1 section of lumbar spinal cord (a) of same animal as in panel B. One box was placed over dorsal V3 INs and another placed over ventral V3 INs. These ROIs were zoomed in on to show double

labelling of CTBA488$^+$ and dsRED$^+$ (b-d for dorsal ROI) and (e-g for ventral ROI). **Scale** = 125 μm. D) L6 section of lumbar spinal cord (a) from same animal as in panel B. **Scale** = 500 μm. One box was placed over intermediate V3 INs. This ROIs was zoomed in on to show double labelling of CTBA488$^+$ and dsRED$^+$ (b-d). **Scale** = 125 μm. E) Midline unilateral (n = 3 injections) and right unilateral grey matter (n = 1 injection) injections demonstrated that dorsal, intermediate and ventral V3 INs ipsilateral and contralateral to injection sites were CTBA488$^+$/dsRED$^+$ throughout the lumbar spinal cord (n = 9 – 10 sections per mouse).

Figure 5. Channel rhodopsin expression in lumbar V3 neurons and nerve terminals in the IML. A) Cross section images of L2 spinal cord demonstrating V3 neurons (TdTomato, Ai) expressing channel rhodopsin (Aii) and merged in panel Aiii. B) Cross section images of T6 spinal cord expressing Tdtomato (Bi) and channel rhodopsin (Bii) and merged in panel Biii. Square highlighting high expression of Tdtomato and channel rhodopsin expression in thoracic IML. C) Optical stimulation evokes multiple action potential in whole-cell patched clamp V3 neurons. Example from n= 10 cells from 6 mice of both sexes.

Figure 6. Optical stimulation of V3 nerve terminals elicits excitatory post synaptic responses in thoracic SPNs. Optical stimulation of V3 nerve terminals could elicit EPSPs (A, n=2) or action potentials (B, n=4) in whole cell patched clamped thoracic SPNs. Examples from n= 10 cells from 4 mice of both sexes.

Figure 7. Optical stimulation of lumbar V3 neurons elicits action potentials in thoracic SPNs. In whole spinal cord preparation, RDA$^+$ thoracic SPNs were visualized under fluorescence and whole cell patch clamp recordings were collected in response to optical stimulation of the L2 ventral surface. In this example, lumbar V3 stimulation consistently

evoked action potentials in the patched SPN. Example from n =20 cells from 15 mice of both sexes.

REFERENCES

Al-Mosawie A, Wilson JM, Brownstone RM (2007) Heterogeneity of V2-derived interneurons in the adult mouse spinal cord. Eur J Neurosci 26:3003-3015.

Alaynick WA, Jessell TM, Pfaff SL (2011) SnapShot: spinal cord development. Cell 146:178-178 e171.

Bauman WA, Spungen AM (2000) Metabolic changes in persons after spinal cord injury. Phys Med Rehabil Clin N Am 11:109-140.

Bedford TG, Loi PK, Crandall CC (1992) A model of dynamic exercise: the decerebrate rat locomotor preparation. J Appl Physiol (1985) 72:121-127.

Biering-Sorensen B, Kristensen IB, Kjaer M, Biering-Sorensen F (2009) Muscle after spinal cord injury. Muscle Nerve 40:499-519.

Biering-Sorensen F, Bohr HH, Schaadt OP (1990) Longitudinal study of bone mineral content in the lumbar spine, the forearm and the lower extremities after spinal cord injury. Eur J Clin Invest 20:330-335.

Blacklaws J, Deska-Gauthier D, Jones CT, Petracca YL, Liu M, Zhang H, Fawcett JP, Glover JC, Lanuza GM, Zhang Y (2015) Sim1 is required for the migration and axonal projections of V3 interneurons in the developing mouse spinal cord. Dev Neurobiol 75:1003-1017.

Borowska J, Jones CT, Zhang H, Blacklaws J, Goulding M, Zhang Y (2013) Functional subpopulations of V3 interneurons in the mature mouse spinal cord. J Neurosci 33:18553-18565.

Bouvier J, Caggiano V, Leiras R, Caldeira V, Bellardita C, Balueva K, Fuchs A, Kiehn O (2015) Descending Command Neurons in the Brainstem that Halt Locomotion. Cell 163:1191-1203.

Bretzner F, Brownstone RM (2013) Lhx3-Chx10 reticulospinal neurons in locomotor circuits. J Neurosci 33:14681-14692.

Chong RK, Bedford TG (1997) Heart rate, blood pressure, and running speed responses to mesencephalic locomotor region stimulation in anesthetized rats. Pflugers Arch 434:280-284.

Chopek JW, Zhang Y, Brownstone RM (2021) Intrinsic brainstem circuits comprised of Chx10-expressing neurons contribute to reticulospinal output in mice. J Neurophysiol 126:1978-1990.

Chopek JW, Nascimento F, Beato M, Brownstone RM, Zhang Y (2018) Sub-populations of Spinal V3 Interneurons Form Focal Modules of Layered Pre-motor Microcircuits. Cell Rep 25:146-156.e143.

Cowley KC (2018) A new conceptual framework for the integrated neural control of locomotor and sympathetic function: implications for exercise after spinal cord injury. Appl Physiol Nutr Metab 43:1140-1150.

Cowley KC, Zaporozhets E, Schmidt BJ (2008) Propriospinal neurons are sufficient for bulbospinal transmission of the locomotor command signal in the neonatal rat spinal cord. J Physiol 586:1623-1635.
Cowley KC, Zaporozhets E, Schmidt BJ (2010) Propriospinal transmission of the locomotor command signal in the neonatal rat. Ann N Y Acad Sci 1198:42-53.
Crone SA, Zhong G, Harris-Warrick R, Sharma K (2009) In Mice Lacking V2a Interneurons, Gait Depends on Speed of Locomotion. Journal of Neuroscience 29:7098-7109.
Crone SA, Viemari JC, Droho S, Mrejeru A, Ramirez JM, Sharma K (2012) Irregular Breathing in Mice following Genetic Ablation of V2a Neurons. J Neurosci 32:7895-7906.
Crone SA, Quinlan KA, Zagoraiou L, Droho S, Restrepo CE, Lundfald L, Endo T, Setlak J, Jessell TM, Kiehn O, Sharma K (2008) Genetic Ablation of V2a Ipsilateral Interneurons Disrupts Left-Right Locomotor Coordination in Mammalian Spinal Cord. Neuron 60:70-83.
Danner SM, Wilshin SD, Shevtsova NA, Rybak IA (2016) Central control of interlimb coordination and speed-dependent gait expression in quadrupeds. J Physiol 594:6947-6967.
Danner SM, Shevtsova NA, Frigon A, Rybak IA (2017) Computational modeling of spinal circuits controlling limb coordination and gaits in quadrupeds. Elife 6.
Danner SM, Zhang H, Shevtsova NA, Borowska-Fielding J, Deska-Gauthier D, Rybak IA, Zhang Y (2019) Spinal V3 Interneurons and Left-Right Coordination in Mammalian Locomotion. Front Cell Neurosci 13:516.
de Groot S, Post MW, Postma K, Sluis TA, van der Woude LH (2010) Prospective analysis of body mass index during and up to 5 years after discharge from inpatient spinal cord injury rehabilitation. J Rehabil Med 42:922-928.
Duckworth WC, Solomon SS, Jallepalli P, Heckemeyer C, Finnern J, Powers A (1980) Glucose intolerance due to insulin resistance in patients with spinal cord injuries. Diabetes 29:906-910.
Eldridge FL, Millhorn DE, Waldrop TG (1981) Exercise hyperpnea and locomotion: parallel activation from the hypothalamus. Science 211:844-846.
Flett S, Garcia J, Cowley KC (2022a) Spinal electrical stimulation to improve sympathetic autonomic functions needed for movement and exercise after spinal cord injury: a scoping clinical review. J Neurophysiol 128:649-670.
Flett S, Garcia J, Cowley KC (2022b) Spinal electrical stimulation for restoration of autonomic functions needed for movement and exercise after spinal cord injury: a systemic scoping review. J Neurophysiology accepted.
Jensen I, Llewellyn-Smith IJ, Pilowsky P, Minson JB, Chalmers J (1995) Serotonin inputs to rabbit sympathetic preganglionic neurons projecting to the superior cervical ganglion or adrenal medulla. J Comp Neurol 353:427-438.
Jessell TM (2000) Neuronal specification in the spinal cord: inductive signals and transcriptional codes. Nat Rev Genet 1:20-29.
Juvin L, Le Gal JP, Simmers J, Morin D (2012) Cervicolumbar coordination in mammalian quadrupedal locomotion: role of spinal thoracic circuitry and limb sensory inputs. J Neurosci 32:953-965.
Kerman IA (2008) Organization of brain somatomotor-sympathetic circuits. Exp Brain Res 187:1-16.

Kerman IA, Akil H, Watson SJ (2006) Rostral elements of sympatho-motor circuitry: a virally mediated transsynaptic tracing study. J Neurosci 26:3423-3433.
Kerman IA, Enquist LW, Watson SJ, Yates BJ (2003) Brainstem substrates of sympatho-motor circuitry identified using trans-synaptic tracing with pseudorabies virus recombinants. J Neurosci 23:4657-4666.
Kerman IA, Bernard R, Rosenthal D, Beals J, Akil H, Watson SJ (2007) Distinct populations of presympathetic-premotor neurons express orexin or melanin-concentrating hormone in the rat lateral hypothalamus. J Comp Neurol 505:586-601.
Kiehn O (2016) Decoding the organization of spinal circuits that control locomotion. Nat Rev Neurosci 17:224-238.
Koba S, Yoshida T, Hayashi N (2005) Sympathetically induced renal vasoconstriction during stimulation of mesencephalic locomotor region in rats. Auton Neurosci 121:40-46.
Koba S, Kumada N, Narai E, Kataoka N, Nakamura K, Watanabe T (2022) A brainstem monosynaptic excitatory pathway that drives locomotor activities and sympathetic cardiovascular responses. Nature Communications 13:5079.
Krukoff TL, Ciriello J, Calaresu FR (1985) Segmental distribution of peptide- and 5HT-like immunoreactivity in nerve terminals and fibers of the thoracolumbar sympathetic nuclei of the cat. The Journal of comparative neurology 240:103-116.
Lanuza GM, Gosgnach S, Pierani A, Jessell TM, Goulding M (2004) Genetic identification of spinal interneurons that coordinate left-right locomotor activity necessary for walking movements. Neuron 42:375-386.
Le Gal JP, Juvin L, Cardoit L, Morin D (2016) Bimodal Respiratory-Locomotor Neurons in the Neonatal Rat Spinal Cord. J Neurosci 36:926-937.
Llewellyn-Smith IJ (2009) Anatomy of synaptic circuits controlling the activity of sympathetic preganglionic neurons. J Chem Neuroanat 38:231-239.
Llewellyn-Smith IJ, Phend KD, Minson JB, Pilowsky PM, Chalmers JP (1992) Glutamate-immunoreactive synapses on retrogradely-labelled sympathetic preganglionic neurons in rat thoracic spinal cord. Brain Res 581:67-80.
Llewellyn-Smith IJ, Martin CL, Fenwick NM, Dicarlo SE, Lujan HL, Schreihofer AM (2007) VGLUT1 and VGLUT2 innervation in autonomic regions of intact and transected rat spinal cord. J Comp Neurol 503:741-767.
Lundfald L, Restrepo CE, Butt SJ, Peng CY, Droho S, Endo T, Zeilhofer HU, Sharma K, Kiehn O (2007) Phenotype of V2-derived interneurons and their relationship to the axon guidance molecule EphA4 in the developing mouse spinal cord. Eur J Neurosci 26:2989-3002.
Moran-Rivard L, Kagawa T, Saueressig H, Gross MK, Burrill J, Goulding M (2001) Evx1 is a postmitotic determinant of v0 interneuron identity in the spinal cord. Neuron 29:385-399.
Noonan VK, Fingas M, Farry A, Baxter D, Singh A, Fehlings MG, Dvorak MF (2012) Incidence and prevalence of spinal cord injury in Canada: a national perspective. Neuroepidemiology 38:219-226.
Pierani A, Moran-Rivard L, Sunshine MJ, Littman DR, Goulding M, Jessell TM (2001) Control of interneuron fate in the developing spinal cord by the progenitor homeodomain protein Dbx1. Neuron 29:367-384.
Rybak IA, Dougherty KJ, Shevtsova NA (2015) Organization of the Mammalian Locomotor CPG: Review of Computational Model and Circuit Architectures Based on Genetically Identified Spinal Interneurons(1,2,3). eNeuro 2.

Schwenkgrub J, Harrell ER, Bathellier B, Bouvier J (2020) Deep imaging in the brainstem reveals functional heterogeneity in V2a neurons controlling locomotion. Sci Adv 6.
Szokol K, Glover JC, Perreault MC (2008) Differential origin of reticulospinal drive to motoneurons innervating trunk and hindlimb muscles in the mouse revealed by optical recording. J Physiol 586:5259-5276.
Talpalar AE, Bouvier J, Borgius L, Fortin G, Pierani A, Kiehn O (2013) Dual-mode operation of neuronal networks involved in left-right alternation. Nature 500:85-88.
Usseglio G, Gatier E, Heuzé A, Hérent C, Bouvier J (2020) Control of Orienting Movements and Locomotion by Projection-Defined Subsets of Brainstem V2a Neurons. Current Biology.
Zagoraiou L, Akay T, Martin JF, Brownstone RM, Jessell TM, Miles GB (2009) A cluster of cholinergic premotor interneurons modulates mouse locomotor activity. Neuron 64:645-662.
Zhang H, Shevtsova NA, Deska-Gauthier D, Mackay C, Dougherty KJ, Danner SM, Zhang Y, Rybak IA (2022) The role of V3 neurons in speed-dependent interlimb coordination during locomotion in mice. Elife 11.
Zhang Y, Narayan S, Geiman E, Lanuza GM, Velasquez T, Shanks B, Akay T, Dyck J, Pearson K, Gosgnach S, Fan CM, Goulding M (2008) V3 spinal neurons establish a robust and balanced locomotor rhythm during walking. Neuron 60:84-96.
Ziskind-Conhaim L, Hochman S (2017) Diversity of molecularly defined spinal interneurons engaged in mammalian locomotor pattern generation. J Neurophysiol 118:2956-2974.

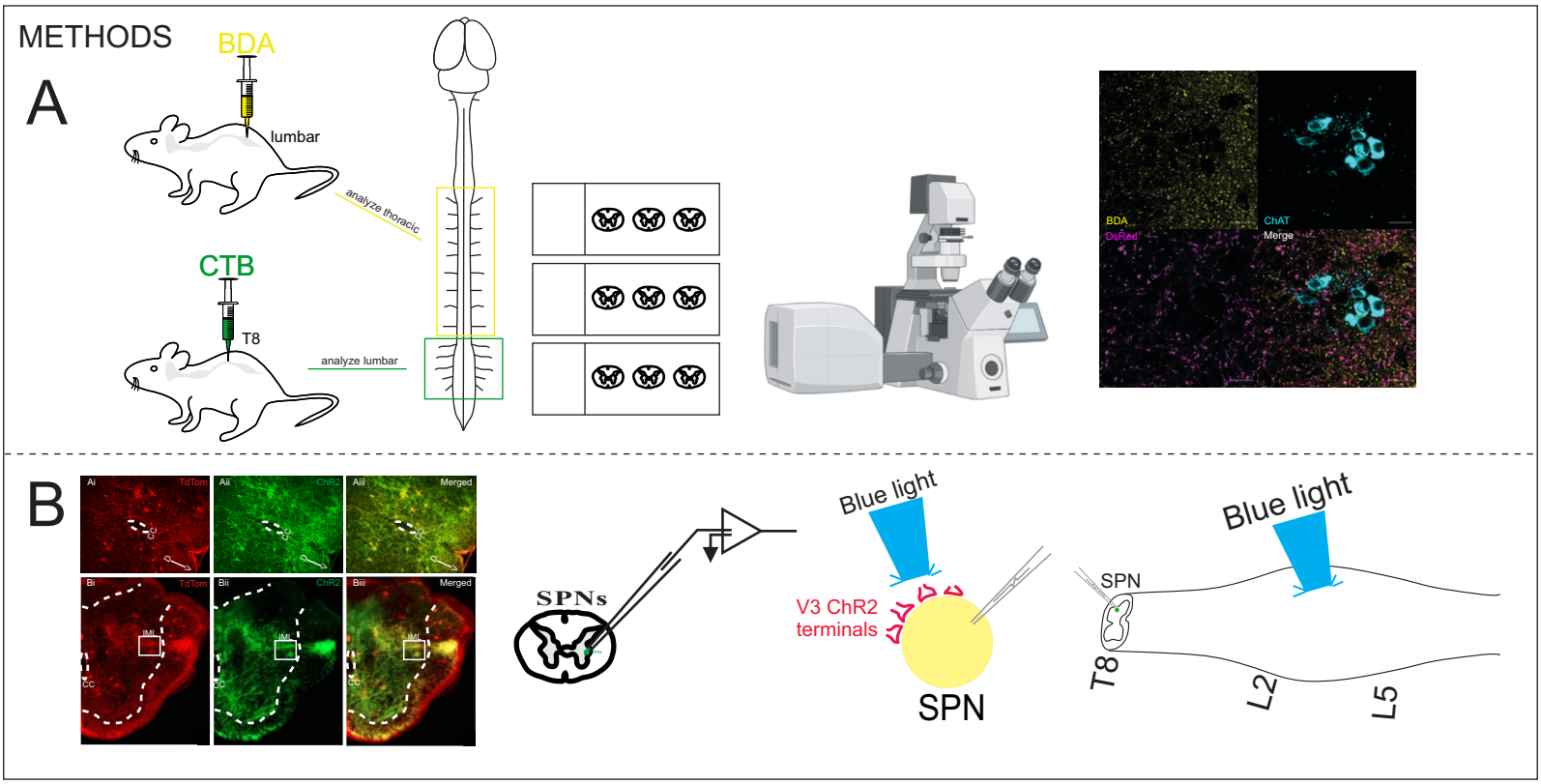
METHODS
A
BDA
lumbar
analyze thoracic
CTB
T8
analyze lumbar
BDA
DsRed
ChAT
Merge
B
Ai
TdTom
Aii
ChR2
Aiii
Merged
Bi
Bii
Biii
IML
CC
SPNs
Blue light
V3 ChR2
terminals
SPN
Blue light
SPN
T8
L2
L5

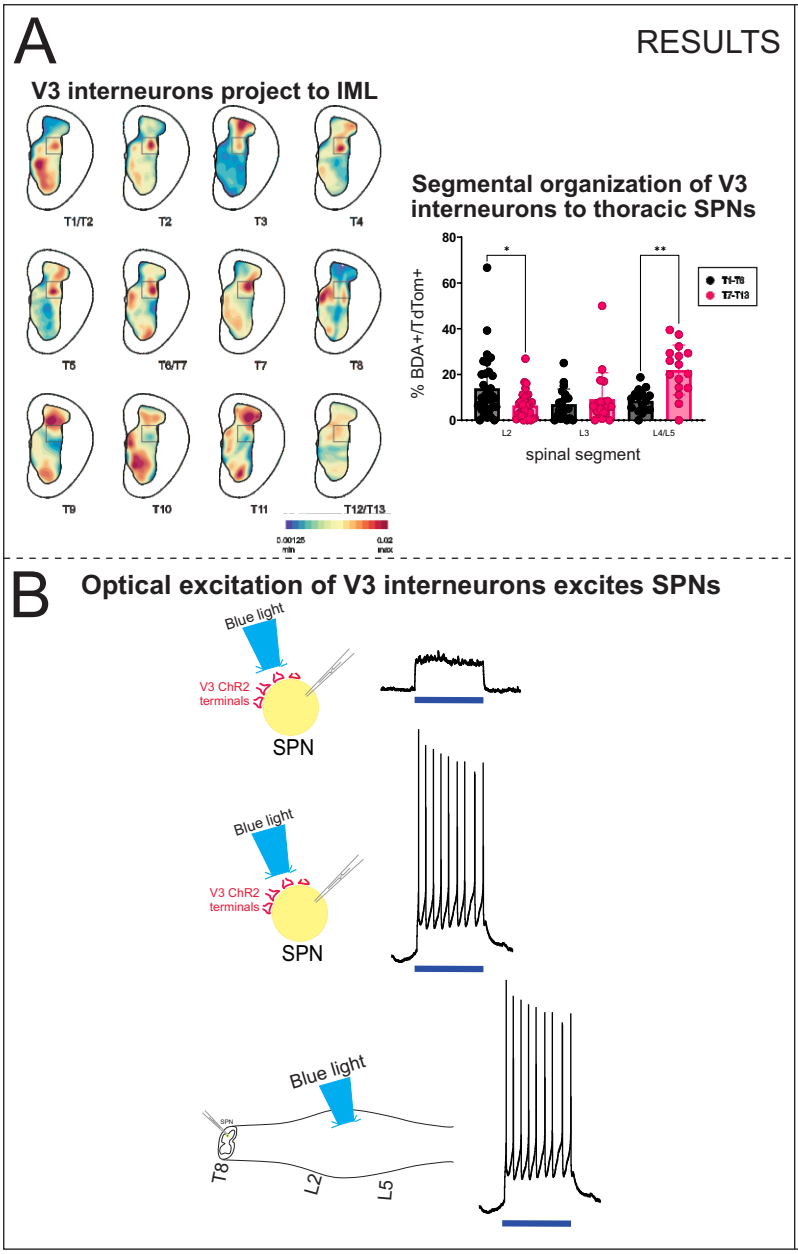
A
RESULTS
V3 interneurons project to IML
T1/T2
T2
T3
T4
T5
T6/T7
T7
T8
T9
T10
T11
T12/T13
0.00125
min
0.02
max
Segmental organization of V3 interneurons to thoracic SPNs
% BDA+/TdTom+
80
60
40
20
0
*
**
T1-T6
T7-T13
L2
L3
L4/L5
spinal segment
B
Optical excitation of V3 interneurons excites SPNs
Blue light
V3 ChR2
terminals
SPN
Blue light
V3 ChR2
terminals
SPN
Blue light
T8
L2
L5

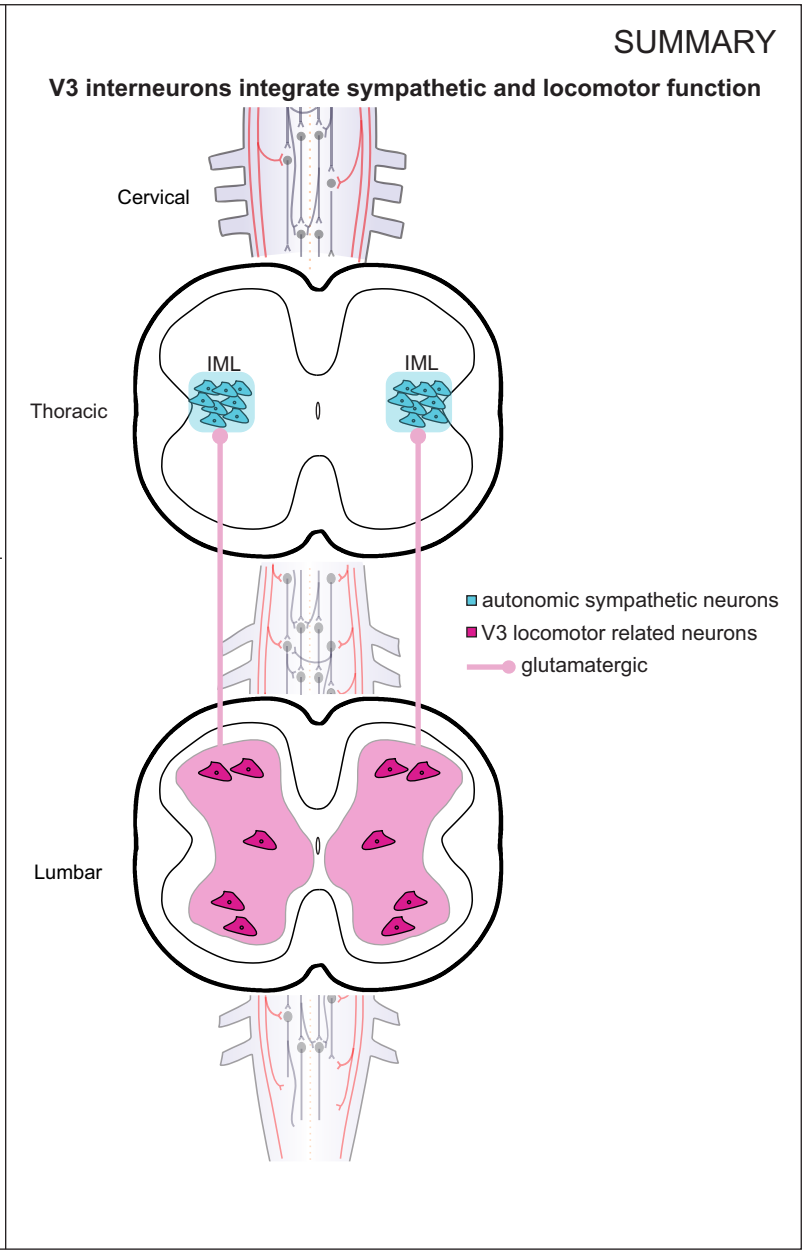
SUMMARY
V3 interneurons integrate sympathetic and locomotor function
Cervical
Thoracic
IML
IML
Lumbar
autonomic sympathetic neurons
V3 locomotor related neurons
glutamatergic

A

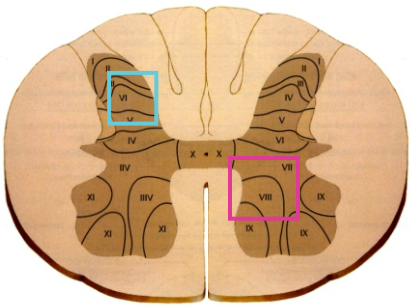

B

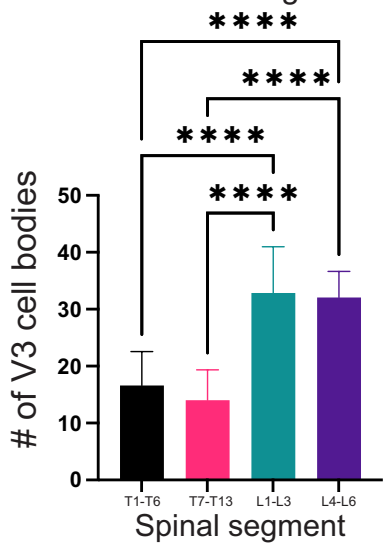
V3 cell bodies throughout spinal cord
****
****
****
****
# of V3 cell bodies
50
40
30
20
10
0
T1-T6
T7-T13
L1-L3
L4-L6
Spinal segment

C

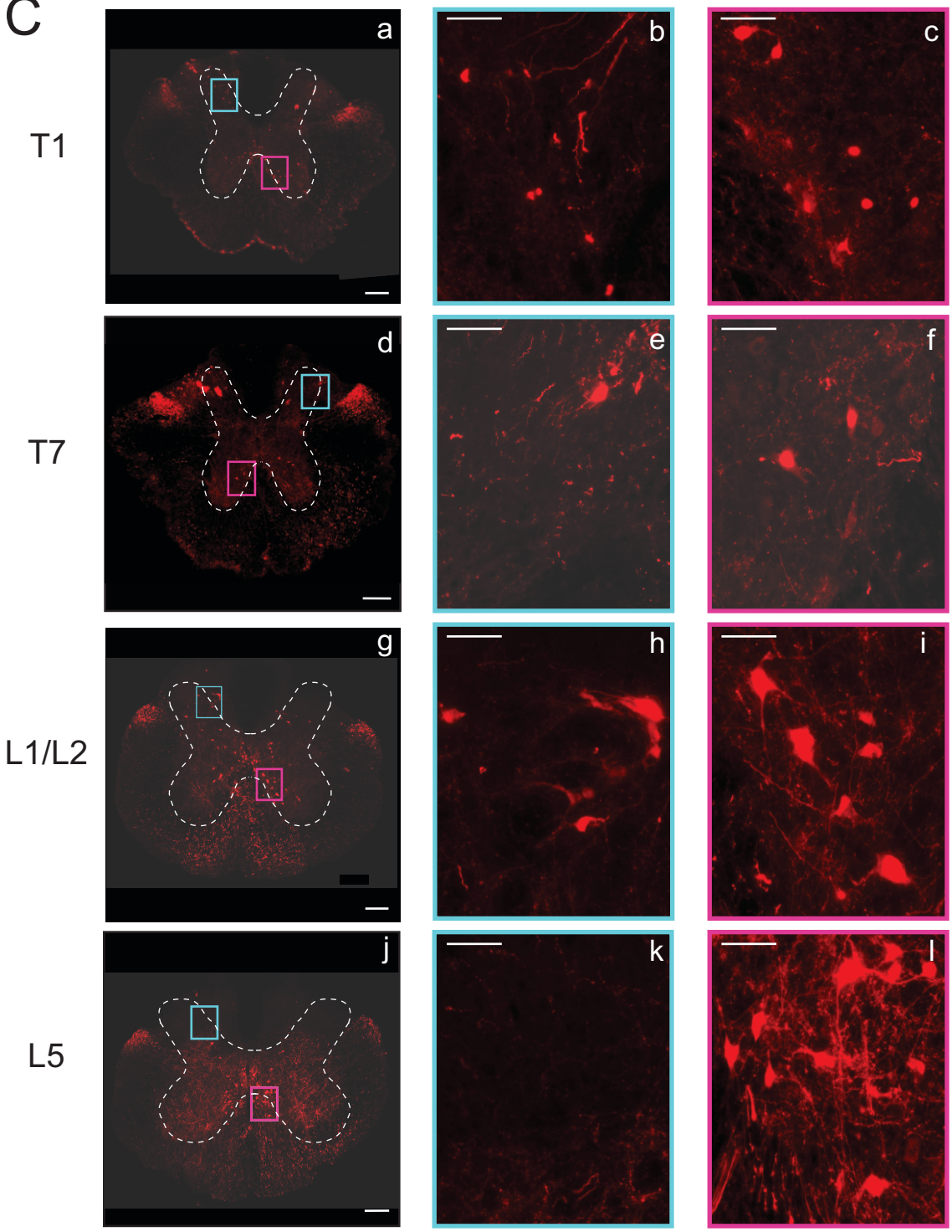
T1
T7
L1/L2
L5
a
b
c
d
e
f
g
h
i
j
k
l

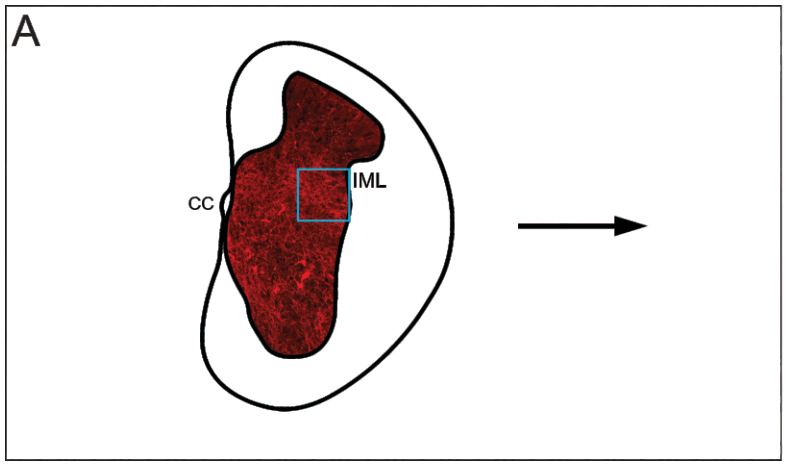
A
CC
IML

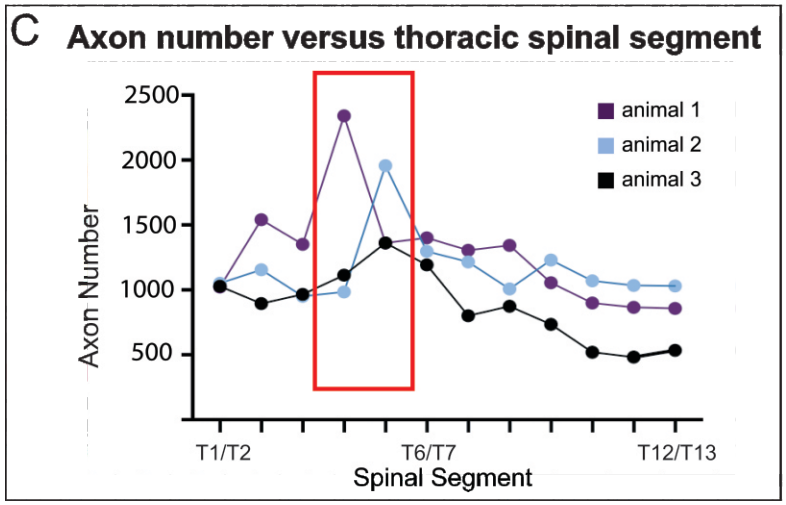
C
Axon number versus thoracic spinal segment
2500
2000
1500
1000
500
Axon Number
animal 1
animal 2
animal 3
T1/T2
T6/T7
T12/T13
Spinal Segment

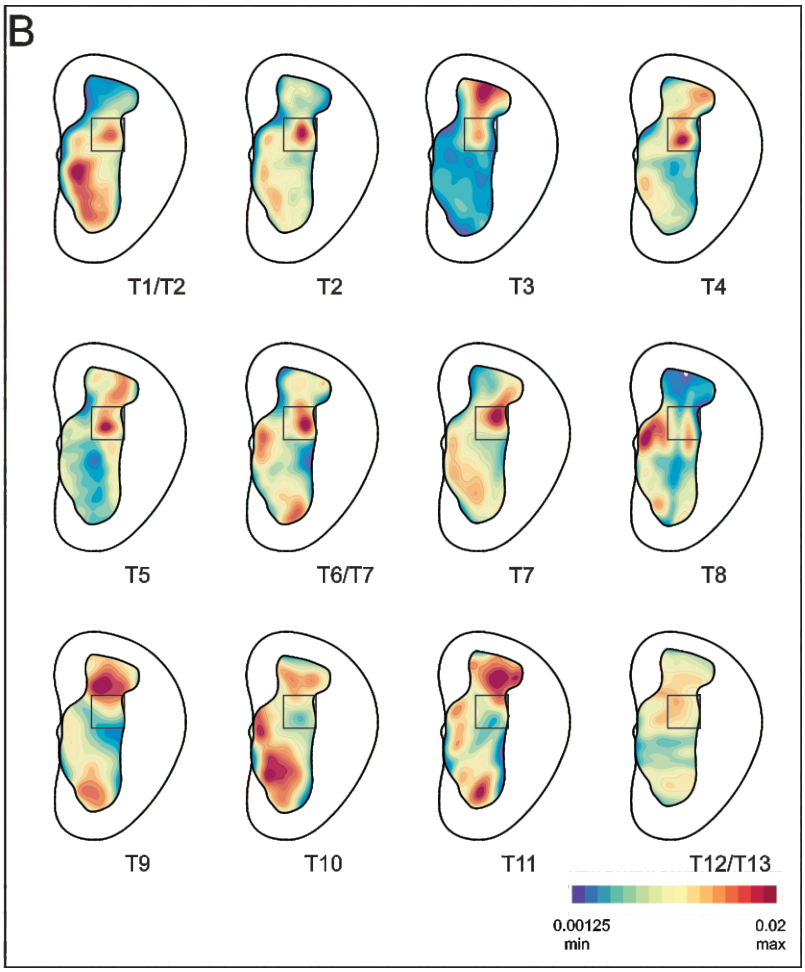
B
T1/T2
T2
T3
T4
T5
T6/T7
T7
T8
T9
T10
T11
T12/T13
0.00125
min
0.02
max

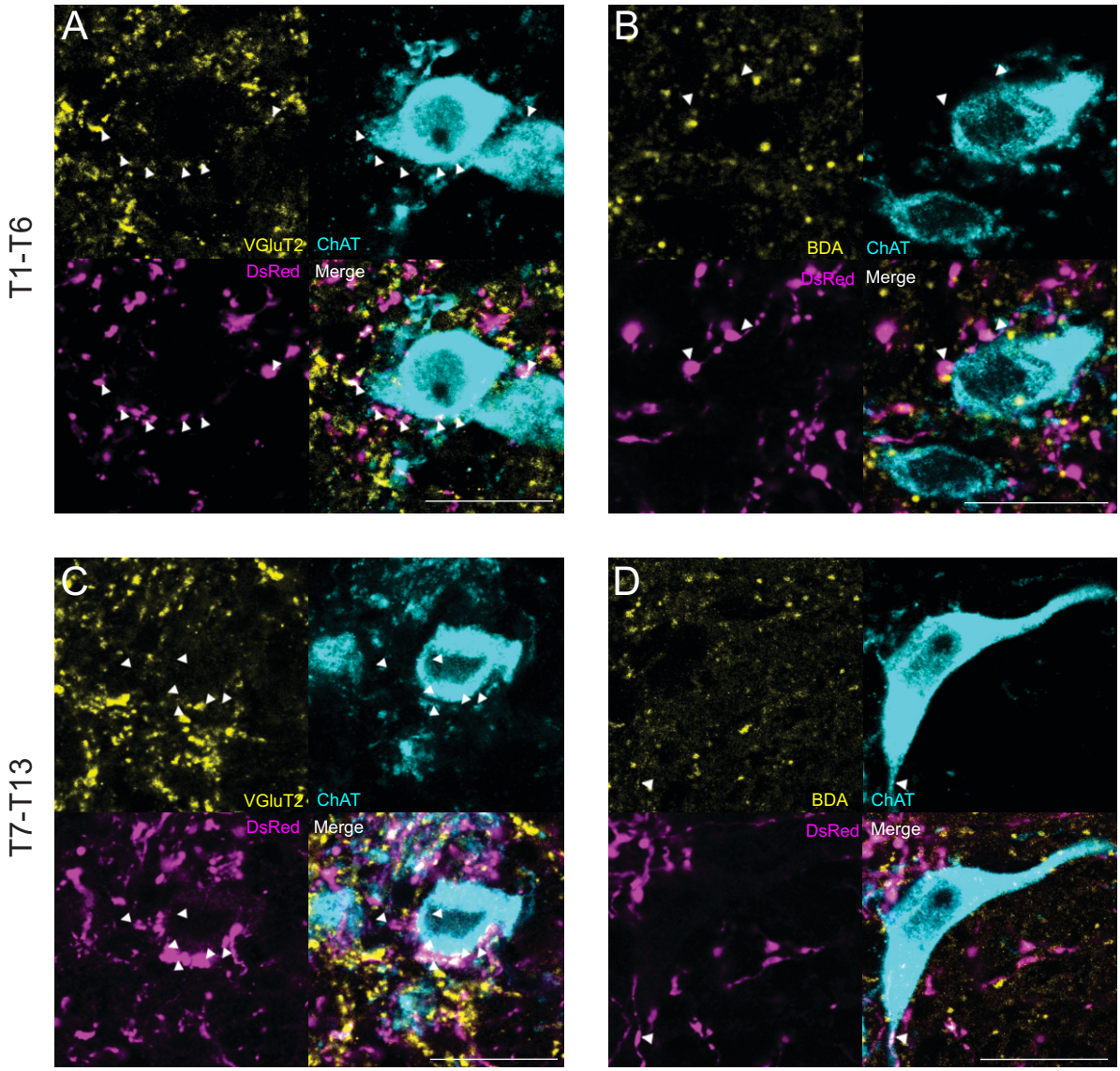

E

Rostrocaudal distribution of double labelled puncta

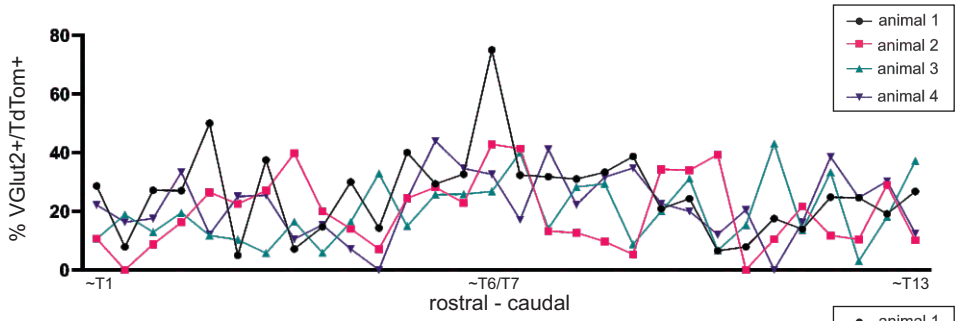

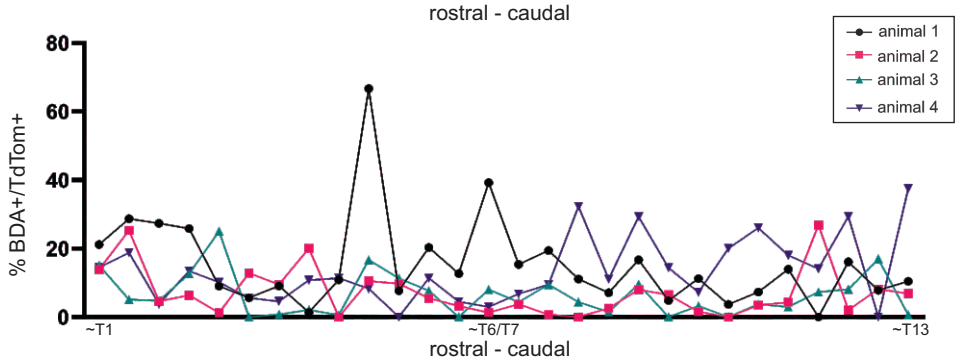

Excitatory V3 innervation on SPNs

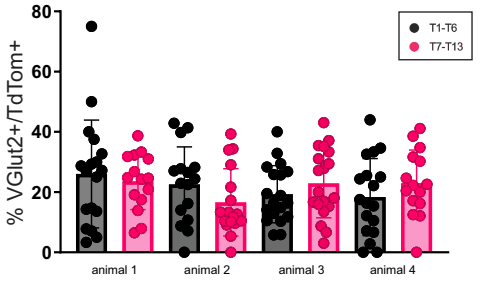

Segmental organization of V3 INs

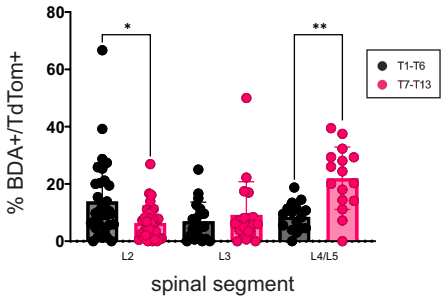

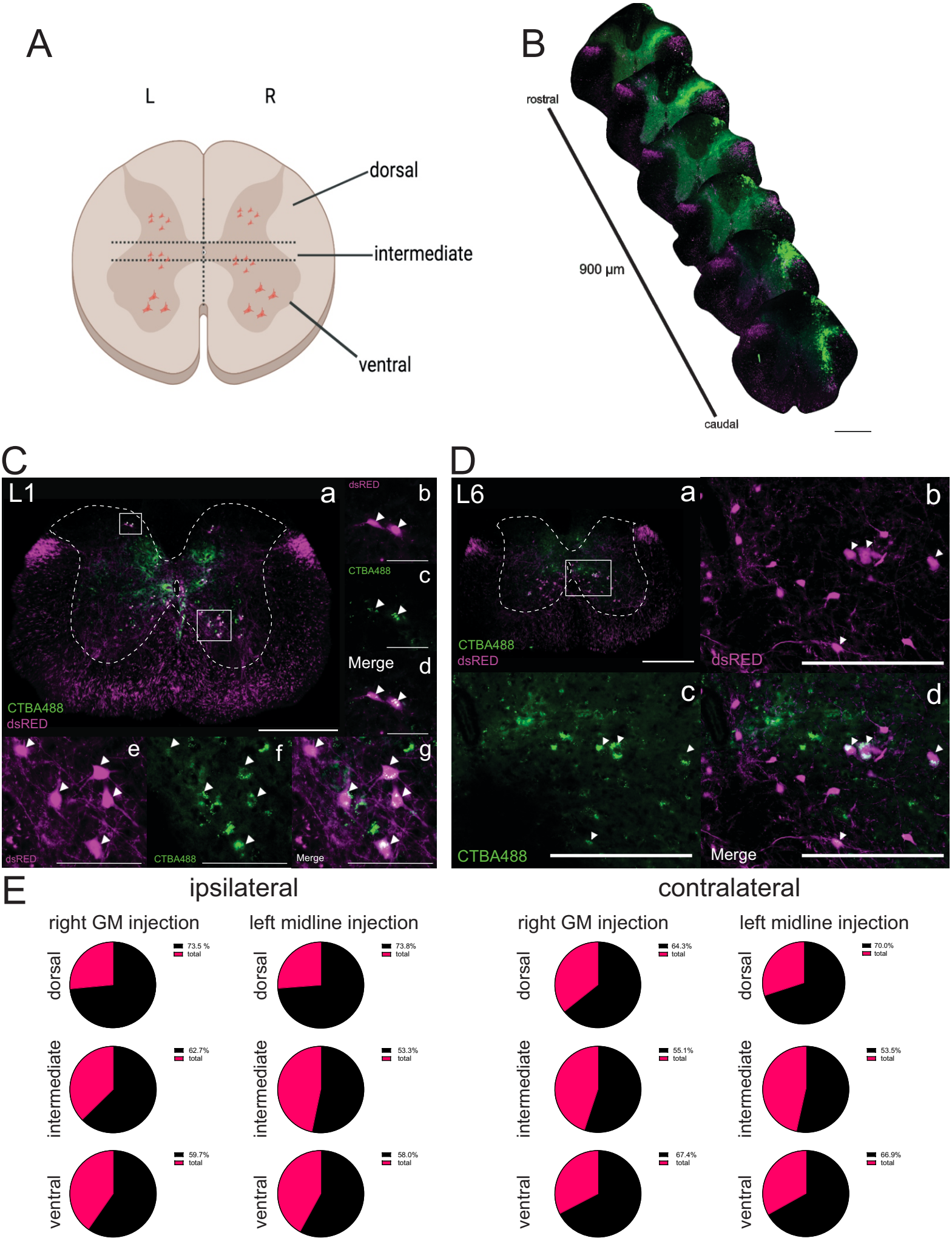
A
L
R
dorsal
intermediate
ventral
B
rostral
900 µm
caudal
C
L1
a
b
dsRED
c
CTBA488
d
Merge
CTBA488
dsRED
e
f
g
dsRED
CTBA488
Merge
D
L6
a
b
CTBA488
dsRED
dsRED
c
d
CTBA488
Merge
E
ipsilateral
contralateral
right GM injection
left midline injection
right GM injection
left midline injection
dorsal
intermediate
ventral
73.5 %
total
62.7%
total
59.7%
total
73.8%
total
53.3%
total
58.0%
total
64.3%
total
55.1%
total
67.4%
total
70.0%
total
53.5%
total
66.9%
total

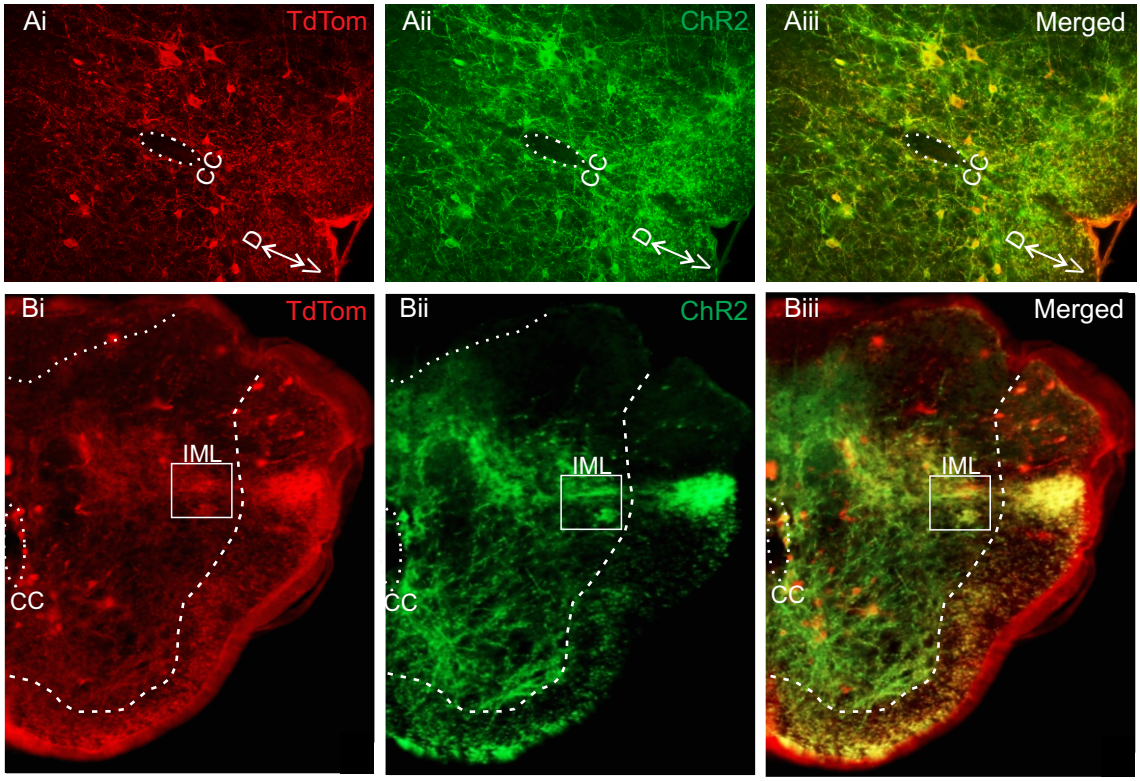
Ai
TdTom
CC
D
Aii
ChR2
CC
D
Aiii
Merged
CC
D
Bi
TdTom
IML
CC
Bii
ChR2
IML
CC
Biii
Merged
IML
CC

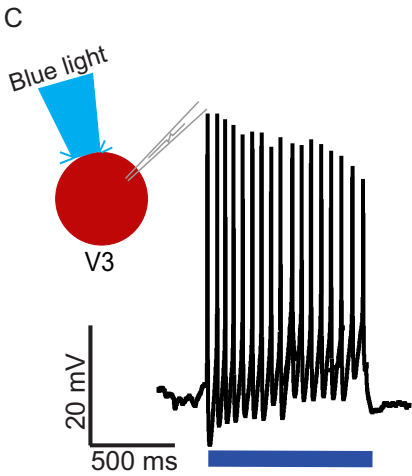
C
Blue light
V3
20 mV
500 ms

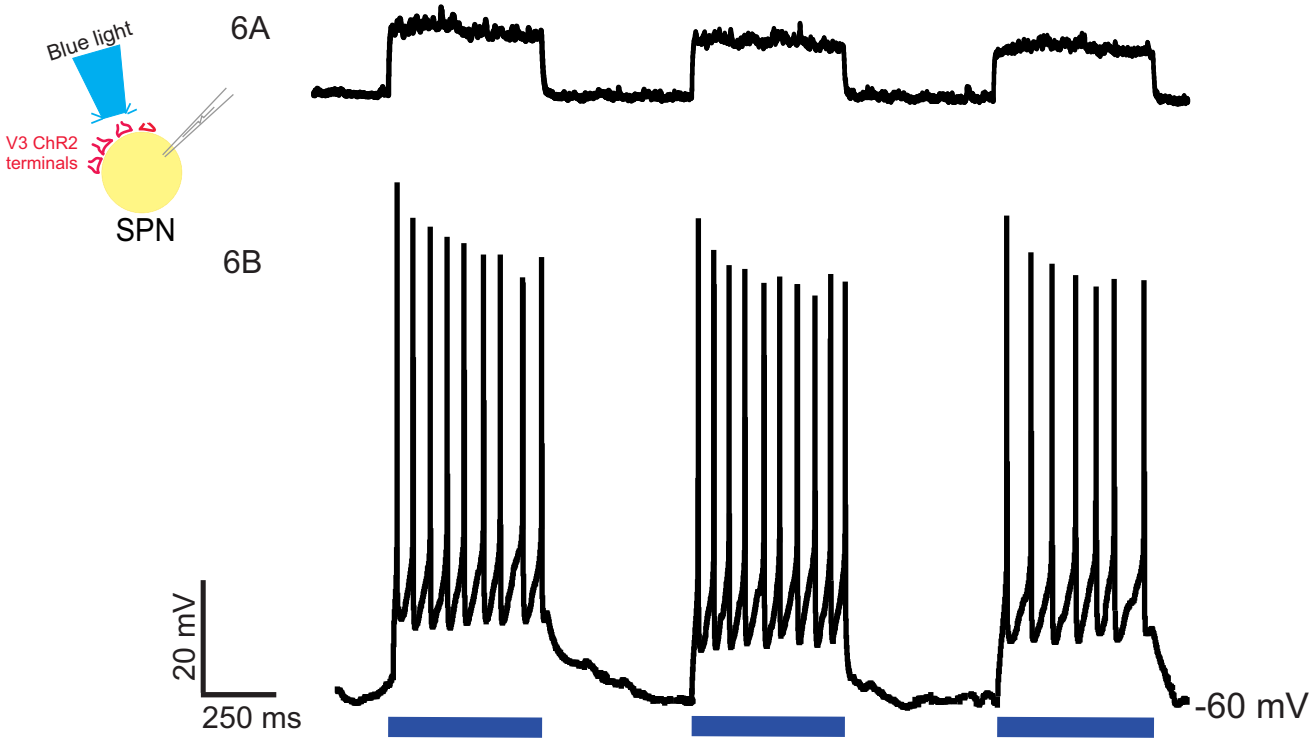
Blue light
V3 ChR2
terminals
SPN
6A
6B
20 mV
250 ms
-60 mV

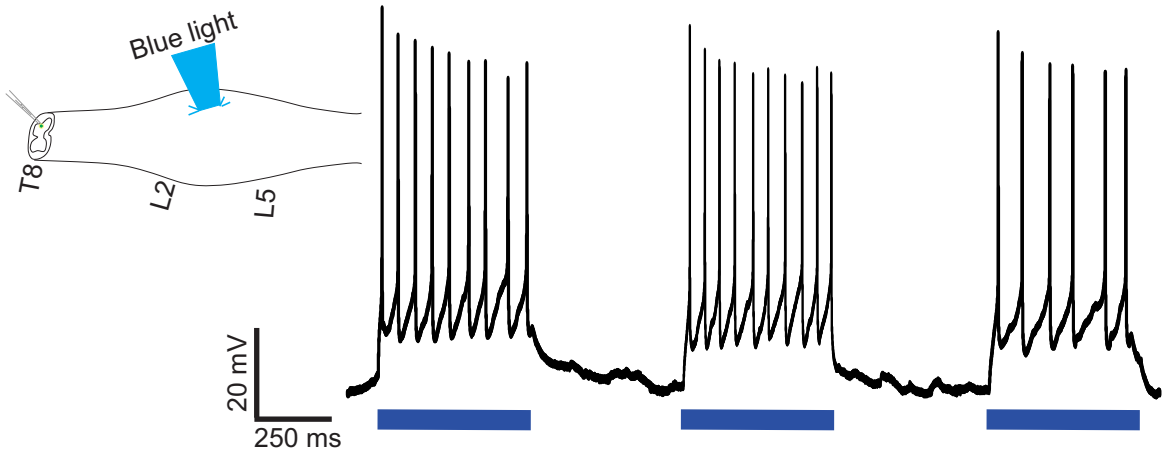
Blue light
T8
L2
L5
20 mV
250 ms